# Size-Resolved Kinetic Measurements of Aluminum Nanoparticle Oxidation with Single Particle Mass Spectrometry

### K. Park, D. Lee,[†] A. Rai, D. Mukherjee, and M. R. Zachariah*

*Center for NanoEnergetics Research, Departments of Chemistry and Mechanical Engineering, University of Maryland, College Park, Maryland 20852*

*Received: May 7, 2004; In Final Form: November 9, 2004*

Aluminum nanoparticles are being considered as a possible fuel in advanced energetic materials application. Of considerable interest therefore is a knowledge of just how reactive these materials are, and what the effect of size on reactivity is. In this paper we describe results of size resolved oxidation rate using a recently developed quantitative single particle mass spectrometer (SPMS). Aluminum nanoparticles used were either generated by DC Arc discharge or laser ablation, or by use of commercial aluminum nanopowders. These particles were oxidized in an aerosol flow reactor in air for specified various temperatures (25–1100 °C), and subsequently sampled by the SPMS. The mass spectra obtained were used to quantitatively determine the elemental composition of individual particles and their size. We found that the reactivity of aluminum nanoparticles is enhanced with decreasing primary particle size. Aluminum nanoparticles produced from the DC Arc, which produced the smallest primary particle size (∼19 nm), were found to be the most reactive (∼68% aluminum nanoparticles completely oxidized to aluminum oxide at 900 °C). In contrast, nanopowders with primary particle size greater than ∼50 nm were not fully oxidized even at 1100 °C (∼4%). The absolute rates observed were found to be consistent with an oxide diffusion controlled rate-limiting step. We also determined the size-dependent diffusion-limited rate constants and Arrehenius parameters (activation energy and pre-exponential factor). We found that as the particle size decreases, the rate constant increases and the activation energy decreases. This work provides a quantification of the known pyrophoric nature of fine metal particles.

## I. Introduction

Aluminum nanoparticles are receiving considerable interest lately as a possible approach to enhance the energy release from energetic materials. It is well-known that fine metal particles are highly reactive and in many cases pyrophoric; however, quantification of reactivity has not been extensively explored. Ivanov et al.[1] reported that by adding aluminum nanoparticles in a propellant formulation, the burning rate could be enhanced by a factor of 5–10. Aumann et al.[2] showed that the activation energy for oxidation of aluminum nanopowder with the average diameter of 24–65 nm was much smaller than that for bulk aluminum samples. However, most measurements of condensed-phase reaction kinetics for aluminum particles have been carried out by dynamic thermal techniques such as thermogravimetry (TG) and differential thermal analysis (DTA) that use bulk samples of aluminum nanoparticles, and it is well-known that those techniques suffer from sampling artifacts associated with mass and heat transfer effects.[3,4] Ideally one would like to explore the intrinsic reactivity of nanoparticles in the absence of other rate limiting kinetic effects associated with heat and mass transfer. Ideally this would be an isolated particle exposed to a reactant, and without the possibility of experimental artifacts that may arise from particle–surface interactions.

Recently we reported on development of a quantitative single-particle mass spectrometer, which was employed to determine the thermal decomposition kinetics of metal nitrate aerosols.[4]

In that study we compared the rate obtained from the SPMS with that obtained from TGA and found that the rate obtained from the SPMS could be several orders of magnitude faster. That study concluded that the use of a very small sample, in this case less than 2 fg (∼100 nm particle), allowed us to probe the intrinsic kinetics more quantitatively.

Here, we employ essentially the same approach to determine the reaction kinetics of single aluminum nanoparticles exposed to air at various temperatures and extract Arrehenius-type kinetics as a function of particle size.

## II. Experimental Approach

There are three experimental components to this study. First we need to prepare or obtain aluminum nanoparticles either by generation or re-suspension of pre-made powders. Second, we need to expose these particles to a known reactive environment, in this case air at a specified temperature and time. Finally we need a measurement protocol that can detect changes to the particle, in this case by measuring changes in particle composition by single-particle mass spectrometry.

**A. Generation of Aluminum Nanoparticles.** In the present study, various aerosol generation methods were employed to produce aluminum nanoparticles. Schematics of each method are shown in Figure 1a–c. Note that each method generates physically different types of aluminum nanoparticles (e.g., primary particle size in an agglomerate).

Figure 1a shows what we refer to as the DC-arc discharge method. An arc is ignited between two tungsten electrodes which served as the heat source to evaporate aluminum. The negative

* Address correspondence to this author. E-mail: mrz@umd.edu.
† Present address: School of Mechanical Engineering, Pusan National University, 30 Jangjeon, Geumjeong, Busan 609-735, Korea.

Aluminum Nanoparticle Oxidation

*J. Phys. Chem. B, Vol. 109, No. 15, 2005* **7291**
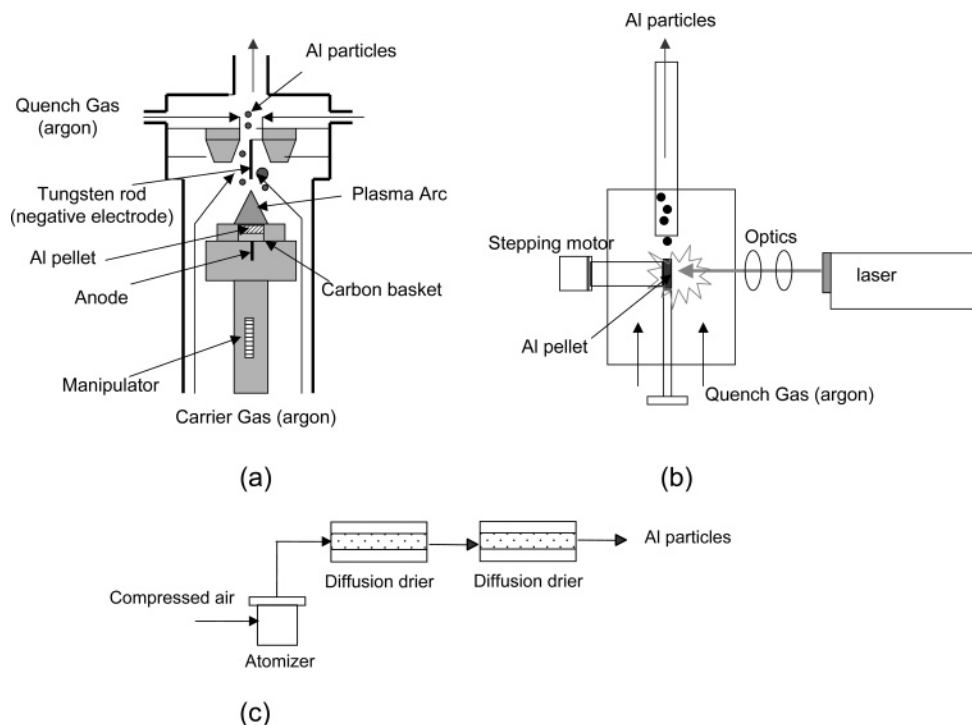


**Figure 1.** Methods used in this study to generate aluminum nanoparticles: (a) DC Arc discharge method, (b) Laser ablation method, and (c) Atomization of commercial aluminum nanopowders.

electrode (cathode) is a tungsten wire clamped between two carbon pieces. A carbon basket with a tungsten rod inserted in the center serves as the anode, and holds aluminum pellets obtained from Sigma-Aldrich Inc. with a purity of 99.99%. An infinite amperes arc welder served as the DC power supply. For the evaporation of aluminum we found we could sustain a stable arc at 15−20 V, and currents of 25−50 Amperes. Argon with a flow rate of 6−7 LPM is used as the carrier gas to carry the evaporating aluminum. Nanoparticles are subsequently created by additional argon quench gas (22−30 LPM).

We also used a laser ablation technique to produce aluminum nanoparticles. As shown in Figure 1b, a 1064 nm Q-switched Nd:YAG laser operating at 10 Hz, and a pulse width of 4 ns, ablated an aluminum target (99.99% pure Sigma-Aldrich Inc.). The pulsed laser beam of nominal diameter 4−5 mm is focused with a fused silica plano-convex lens of focal length 100 mm to a spot diameter of the order of ∼1 mm at the aluminum pellet surface positioned near the focal point of the lens. The focused laser beam has an energy density of approximately $1 \times 10^{10}$ W/cm$^2$. This generates a local microplasma at the surface of the aluminum target resulting in vaporization of aluminum from the plasma volume region at the target surface. The aluminum target was mounted on a rotating shaft of a programmable stepper motor and located at the center of a sealed reactor cell with an inlet at the bottom and an outlet at the top as indicated in Figure 1b. The stopping intervals between the rotations of the stepper motor were chosen to ablate materials without creating a deep crater. We found that with the present arrangement, aluminum nanoparticles could be produced continuously for as long as 2−3 h without any significant variation in the size distribution. A 1 mm tube carrying inert Argon gas at the center of the reactor cell was aligned with the pellet surface and a 1/4 in. S.S tube located right on top of the aluminum pellet led to the outlet of the cell. Argon gas flowing past the pellet swept the ablated material past the surface and also acted as the quenching gas for recondensation to form nanoparticles.

Commercial aluminum nanopowders were also used from Aveka Inc. and Nanotechnologies Inc., by dispersing the powders in methanol, and generating an aerosol using a Collison atomizer as shown in Figure 1c. These particles passed through several carbon black aerosol diffusion driers to remove the solvent.

**B. Aluminum Nanoparticle Oxidation, Sampling, and Physical Characterization.** Aerosols generated by the above methods enter a tube furnace where particles undergo oxidation in air for a given temperature (25−1100 °C) and residence time (∼1 s). A quartz tube with a 1 cm i.d. and 120 cm long was placed in the tube furnace with a heated length of 30 cm. The aerosols from the tube furnace for the given temperature were directly sampled into the single particle mass spectrometer (SPMS) where their elemental composition and size can be determined as a function of the furnace temperature. A differential mobility analyzer (DMA)[5] was placed upstream of the SPMS to send monodisperse aerosols into the SPMS to determine the relationship between particle size and ion signal intensity. Also, the DMA with a condensation particle counter (CPC) was used to measure particle size distribution. We used Transmission Electron Microscopy (TEM) to examine the structure of aluminum particles, including their primary particle size. A 8-stage low-pressure impactor (LPI),[6] with a minimum cut size of 50 nm, and an electrostatic precipitator were used to collect particles on TEM grids for analysis with a JEOL 1210 TEM (accelerating voltage: 40−120 kV, magnification: 50× to 800 000×). For these studies we used 200 mesh copper TEM grids coated with carbon or silicon monoxide films.

**C. Single Particle Mass Spectrometry.** Our primary analytical tool for this work is a single particle mass spectrometer (SPMS) shown in Figure 2. The primary components of the SPMS consist of an aerodynamic lens inlet, three-stage differential vacuum system, a free firing pulsed laser for ionization of a particle, a linear time-of-flight mass spectrometer, and a 500 MHz digital oscilloscope and PC for data acquisition. More details can be found in our previous paper.[4] The key feature of
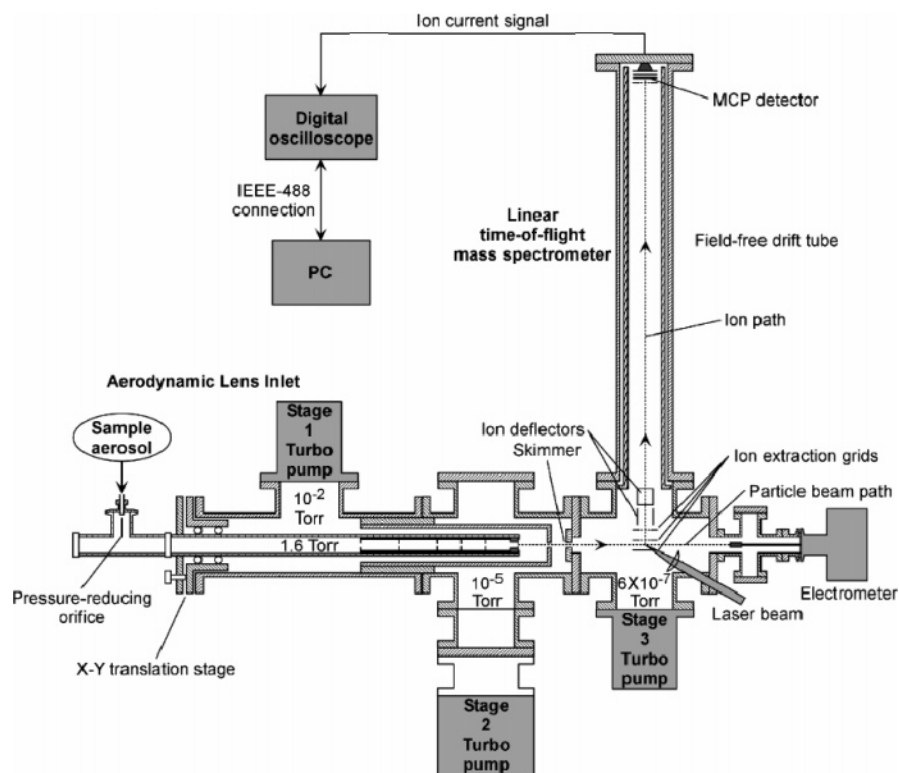
**Figure 2.** Schematic of the single particle mass spectrometer (SPMS).

the instrument is that the use of high fluencies results in *no* molecular ion signals, but a *quantitative* measure of the elemental population in a particle. This very important capability enables us to carry out the kinetics study described in this paper. A brief description is given below.

The aerodynamic lens system is used to produce a narrow collimated particle beam by inertial confinement, and transport particles with a high efficiency into high vacuum system.[7] The free firing pulsed laser (a frequency-doubled Nd:YAG laser operated at 10 Hz, 532 nm wavelength, pulse width ~5 ns) is tightly focused at the extraction field of the mass spectrometer through a 2.5 cm F.L. spherical plano-convex lens and intersects the particle beam, with a laser beam diameter of ~0.3 mm. We operated the laser with a laser energy power above ~100 mJ/ pulse to ensure complete ablation and ionization of the components of a particle. The laser power density at the focal point was estimated to be approximately $1.7 \times 10^{10}$ W/cm$^2$, which roughly corresponds to a factor of 1 million times more energy impinging on the particle than is necessary to completely vaporize and ionize all the elements. The pressure of the mass spectrometer region is ~$10^{-7}$ Torr when the inlet is open. A 1 m time-of-flight tube and microchannel plates (MCP) are used to produce a time-of-flight spectrum, collected with a 500 MHz digital oscilloscope.

Another important aspect of this study is that we can determine the size-resolved reactivity of aluminum nanoparticles with the single particle mass spectrometer. Recent advances in aerosol mass spectrometry have made it possible to simulta- neously determine particle size and qualitative composition.[8-10] For example, a recently developed aerosol time-of-flight mass spectrometer (ATOFMS)[9] provided an efficient method to simultaneously measure size and composition of individual particles. However, this method is generally restricted to particles larger than ~200 nm because of the optical detection limits of smaller particles. In the present study, we employ a complete ionization technique where the total ion signal

produced can be used to infer particle size as well as composi- tion. To our knowledge only the Reents group[10] has employed a similar technique. The ions formed in this way are directly related to the number of atoms present in a particle, allowing us to determine particle size.[10] Since this technique does not rely on light scattering for particle sizing, the size-resolved compositions for very small particles down to ~20 nm can be determined.

## III. Results and Discussion

**A. Quantitative Determination of Elemental Composition and Size of Aerosol Particles by the SPMS.** Figure 3 shows example mass spectra for aluminum nanoparticles exposed to air at ambient (a) and elevated furnace temperatures (b−d) for a given residence time (~1 s). One sees that the mass spectrum shows considerable oxygen in the oxidized particle. The elemental stoichiometry for a given particle is estimated as the ratio of the sum of peak areas of each element, based on our prior work that under high laser powers the ion signal is proportional to the number of ions present in a particle.[4,11]

For completeness we show that for DMA size-selected NaCl and Al particles, peak areas of ions for 70 nm NaCl and 85 nm Al particles are essentially constant with varying laser power as shown in Figure 4. We were careful to ensure that the spectra obtained in Figure 4 were not saturated. This implies that we are achieving near complete ionization of the sample. In addition, since our previous study[4] showed that element stoi- chiometry ratios for various aerosols measured with the SPMS were in good agreement with theoretical values, within ~14%, we believe that near complete ionization was obtained. For the remainder of the work we have used a laser power range of ~100 mJ/pulse. It should be pointed out that even if we are achieving high ionization rate, based on recent numerical simulations which we are preparing for publication, the aggres- siveness of the ionization process does result in ion losses. However, these are relatively species independent.

Aluminum Nanoparticle Oxidation

*J. Phys. Chem. B, Vol. 109, No. 15, 2005* **7293**



(a)



(b)



(c)



(d)
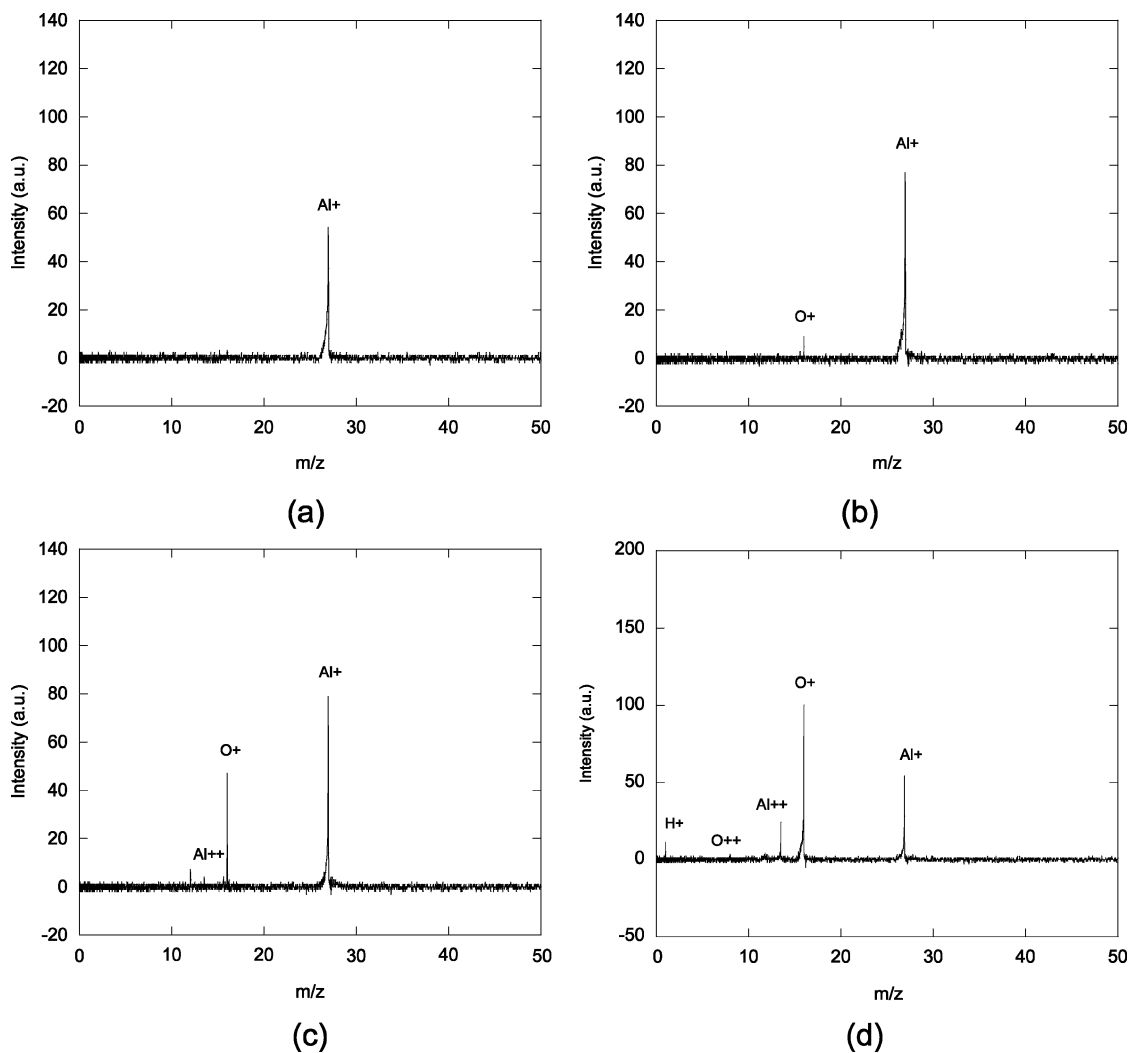
**Figure 3.** Typical mass spectra for the (a) pure aluminum particle, (b and c) partially oxidized aluminum particle, and (d) completely oxidized aluminum particle.
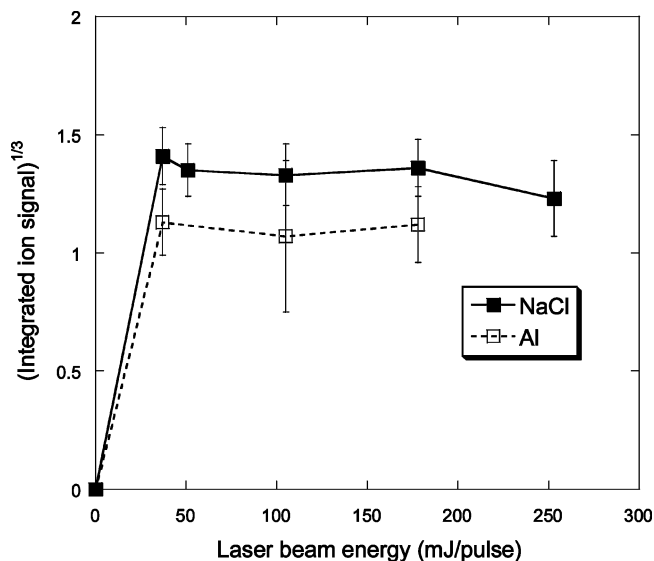


**Figure 4.** The cube root of the integrated ion signals (proportional to diameter) for 70 nm NaCl and 85 nm Al particles as a function of laser power.

Figure 5 shows a distribution of atomic fraction of aluminum (=Al/(Al + O)) for 200 particles exposed to air at the temperature of 1100 °C. Note that the theoretical value of the atomic fraction of aluminum for aluminum oxide ($Al_2O_3$) is 0.4,
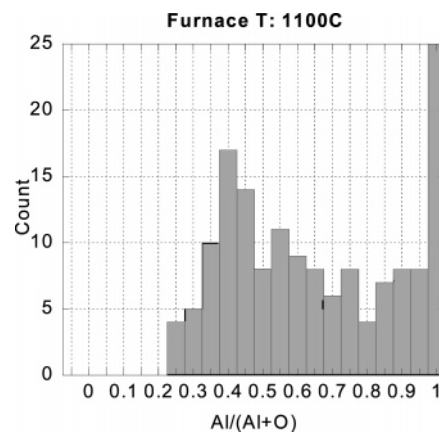


**Figure 5.** Distribution of the atomic fraction of aluminum (Al/(Al+O)) for 200 particles measured with the SPMS at a temperature of 1100 °C.

while the value for pure aluminum (Al) is 1.0. The data suggest that some particles are completely oxidized to aluminum oxide and others are only partially oxidized.

The quantification for particle size from ion signal intensity is based on the idea that the number of atoms present in a particle, which is proportional to peak areas of ions in the mass spectrum, reflects the particle volume that can be used to determine particle size.[10] Reents et al.[10] showed that the variation
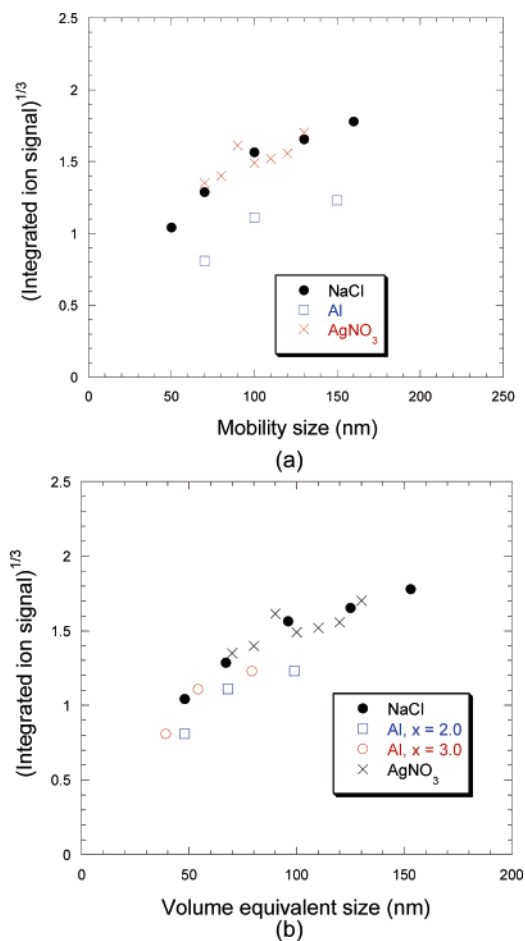
**Figure 6.** Relationship between the integrated ion signal and (a) mobility size ($D_{me}$) and (b) volume equivalent size ($D_{ve}$) after accounting for particle shape ($x$ = dynamic shape factor) for Al particles.

in the number of atoms among different materials is ~30%, allowing only ~10% variation in particle size. This implies that the number of atoms present in the particle can be used to determine particle size independent of particle composition and shape. Using the DMA-generated monodisperse aerosols (NaCl, AgNO₃, and Al), we measured the relationship between the integrated ion signal and particle mobility size (DMA size) as shown in Figure 6a. The difference between two materials might be caused by their different density and shape. Note that Al particles are small agglomerates such that their volume equivalent size is slightly smaller than the mobility equivalent size, while for NaCl particles (cubic shape) the volume equivalent size is close to the mobility size. After accounting for dynamic shape factors for two types of particles ($x$ = 2.0 or 3.0 for Al agglomerate[12]), we obtained the relationship between the integrated ion signal and particle size, based on the volume equivalent size as shown in Figure 6b. This power-law relationship that is relatively independent of particle type implies that the mass spectrum can be used to size particles in addition to characterizing the chemical composition. A more thorough description of the physical basis of the power law relationship can be found elsewhere.[13] Briefly, however, hydrodynamic expansion of the laser induced plasma results in an expanding cloud of ions whose kinetic energy increases with increasing particle size. High kinetic energies decrease the transmission efficiency to the MCP detector and result in the non-linear dependence of total ion signal with particle size. The measured signal is a composite of the ionization efficiency and the ion transmission efficiency. We have estimated by measuring the

MCP current directly that our composite yield accounting for these two effects is ~0.2%. To give the reader a perspective of the role of ion energy on transmission efficiency, a 100 eV singly charged ion of aluminum would be detected with only ~0.1% efficiency in our system. In this study, we used the relationship obtained for Al particles shown in Figure 6a to determine particle size.

**B. Kinetic Measurements of Aluminum Nanoparticle Oxidation.** We obtained isothermal kinetic data for aluminum nanoparticle oxidation by passing them through the tube furnace for a given residence time (~1 s) and temperature (25−1100 °C), and subsequently sampling with the SPMS. The atomic fractions of aluminum (Al/(Al + O)) for 200−300 particles at a given temperature were determined from elemental composition data measured with the SPMS as shown in Figure 5. In our analysis, we introduced the extent of conversion (α) as defined by Levenspiel:[14]

$$\alpha = \text{volume of converted material/total volume of particle} \tag{1}$$

Thus, if the extent of conversion (α) equals 1, a particle is completely oxidized to aluminum oxide (Al₂O₃), while a value of 0 is pure aluminum. Values between 0 and 1, indicate a particle that is partially oxidized, presumably one having an unreacted core (Al) surrounded by an aluminum oxide shell. Using the atomic fraction of aluminum as shown in Figure 5, and information on particle size obtained from the relationship between the integrated ion signal and size, we can calculate the extent of conversion as a function of particle size at each temperature. Figure 7a−d shows the extent of conversion determined in this way for aluminum nanoparticles generated by the DC arc method. Note that as temperature increased, the fraction of particles with α = 1 (i.e., Al₂O₃) increased, and at 900 °C, ~68% of the Al nanoparticles were completely oxidized to Al₂O₃. Also note that the smaller particles oxidized first (i.e. for any given temperature, smaller particles have a larger extent of conversion (α)).

From the data in Figure 7 one can determine the average value for α, which indicates the magnitude in the increase in extent of reaction as a function of temperature shown in Figure 8a. The data can also be binned by size range (<50, 50−100, and 100−150 nm) as seen in Figure 8b. The results present the quantification of the extent to which smaller particles show greater extents of conversion. The reader should be cognizant of the fact that particle size reported represents the mobility size, as DMA-selected particles were used to determine the particle size from the ion signal intensity. We hypothesize that the decreased reactivity with increasing mobility size was caused by a decreased particle surface area-to-volume ratio with an increase in the mobility size. Figure 9a−d shows the morphology of aluminum particles obtained from each source employed in this study. Since the aluminum particles are agglomerates with some extent of "necking" or coalescing spheres, the surface area-to-volume ratio should decrease as the particle mobility size increases. Only agglomerates with a point contact among primary particles have the constant surface area-to-volume ratio, independent of particle mobility size. Further examination is required to determine if indeed the higher reactivity observed for smaller particles is caused mainly by their higher surface area-to-volume ratio. When the values of extent of conversion for particles in the progress of reaction in all sizes are normalized by their surface area-to-volume ratio that was calculated by the mobility size assuming spherical particles, it leads to a similar value (i.e., α/surface area-to-volume ratio = 1.79 for 100−150

Aluminum Nanoparticle Oxidation

*J. Phys. Chem. B, Vol. 109, No. 15, 2005* **7295**
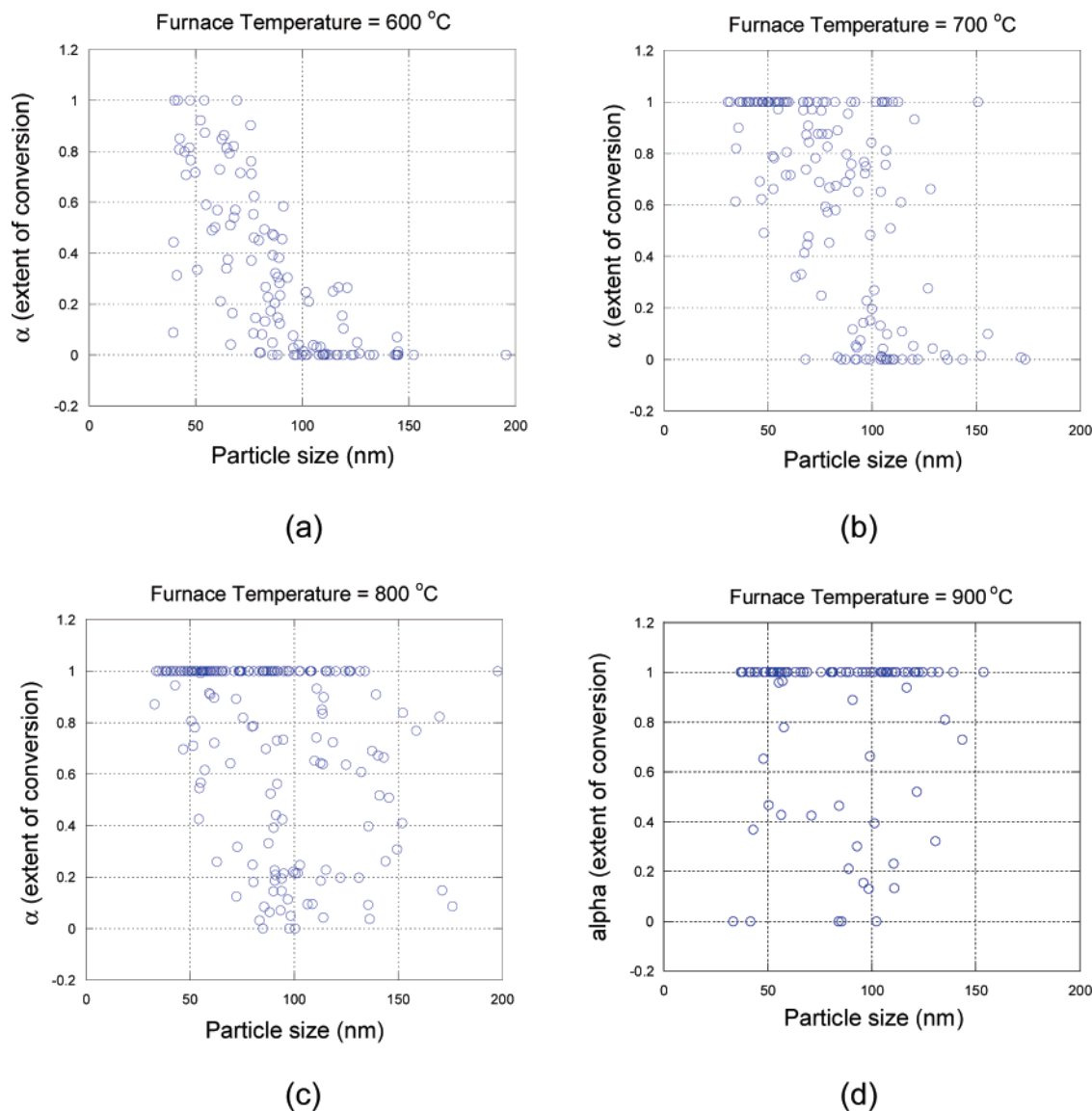


**Figure 7.** The extent of conversion ($\alpha$) as a function of particle size at each temperature for Al nanoparticles produced from the DC arc method: (a) 600, (b) 700, (c) 800, and (d) 900 °C.

nm, 1.82 for 50−100 nm, and 1.71 for <50 nm at 700 °C). This suggests that the enhanced surface area-to-volume ratio with decreasing size plays a major role in the higher reactivity for smaller particles.

Similar measurements were conducted for aluminum nanoparticles generated by other methods. Results for aluminum particles generated from the laser ablation method are shown in Figure 10a−d. We observed that the fraction of oxidized aluminum nanoparticles produced from the laser ablation method at a given temperature is lower than those generated from the DC arc method. All results are summarized in Table 1. It includes the mean size of primary particles that comprise agglomerates measured with the TEM, and the peak mobility size measured with the Scanning Mobility Particle Sizer (SMPS). The peak mobility size was evaluated at the size giving the highest number concentration. We found that the fraction of oxidized aluminum nanoparticles is sensitive to their primary particle size and that the fraction increased with decreasing primary particle size at a given temperature. Aluminum nanoparticles produced from the DC arc that provides primary particles of the smallest (∼19 nm) size were found to be the most reactive (∼68% of particles completely oxidized to

aluminum oxide at 900 °C). In contrast, nanopowders (Nanotechnologies Inc.) with primary particle size greater than 50 nm are not fully oxidized even at 1100 °C (∼4%). This suggests that the primary particle size plays an important role in the reactivity of aluminum nanoparticle agglomerates and that with decreasing primary particle size their reactivity increases.

**C. Kinetic Model for Aluminum Nanoparticle Oxidation.** To obtain a kinetic rate constant from the data, one must first propose a suitable model. We chose the well-known idealized "*shrinking core*" model for spherical particles of unchanging size[14,15] to describe aluminum nanoparticle oxidation. The major approximation being applied in the use of this model is the assumption that the particles are spherical. While we recognize errors may result, we are not able at this time to account for shape effects that vary from particle to particle. This will introduce errors in the interpreted rate constant. The shrinking core model involves a reaction front moving radially inward separating an unreacted core with a completely reacted ash outer layer and is typically described in three steps:

Step 1: Diffusion of gaseous reactant (oxygen) through the film surrounding the particle to particle surface (film resistance).

**(a)**



**(b)**
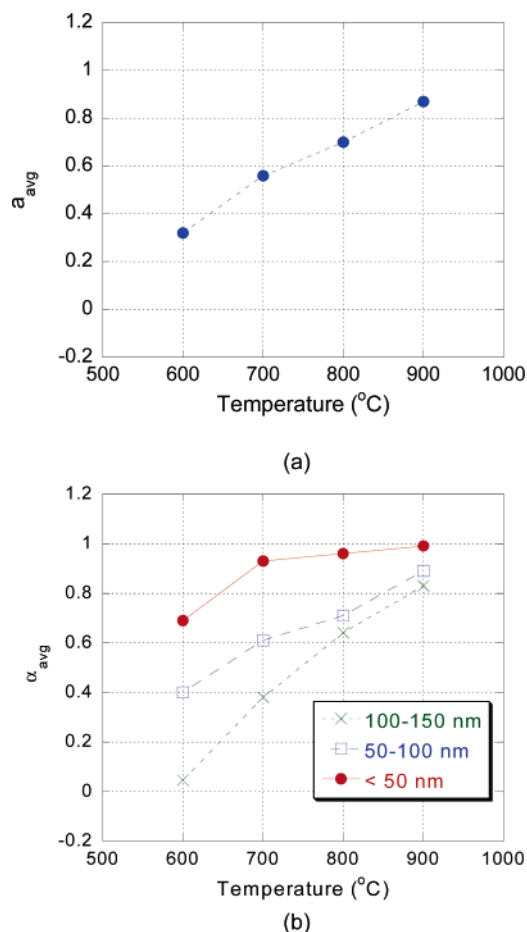
**Figure 8.** (a) Average values of the extent of conversion ($\alpha_{avg}$) in all sizes as a function of temperature. (b) Average values of the extent of conversion ($\alpha_{avg}$) in different size ranges (<50, 50−100, and 100−150 nm) as a function of temperature for Al nanoparticles produced from the DC arc method.



**Figure 9.** Typical morphology of aluminum particles used in this study: (a) DC Arc, (b) laser ablation, (c) Al nanopowder (Aveka Inc.), (d) Al nanopowder (Nanotechnologies Inc.). The TEM image for Al nanopowder from Nanotechnologies Inc. was captured from the company's website.

Step 2: Diffusion of gaseous reactant (oxygen) through the ash (oxide shell) to the surface of unreacted core (aluminum) (ash resistance).

Step 3: Chemical reaction of gaseous reactant (oxygen) with solid (aluminum) at unreacted core surface (chemical reaction resistance).

Since a solid ash (oxide shell) forms very rapidly, the first step (film resistance) can be ignored as a rate-limiting step (i.e., the ash resistance is much greater than the film resistance).[14] This still leaves steps 2 and 3, from which to deduce the rate-limiting step. The time for complete conversion ($\tau$) in each limiting step can be obtained from the extent of conversion ($\alpha$) by the following equations:[14]
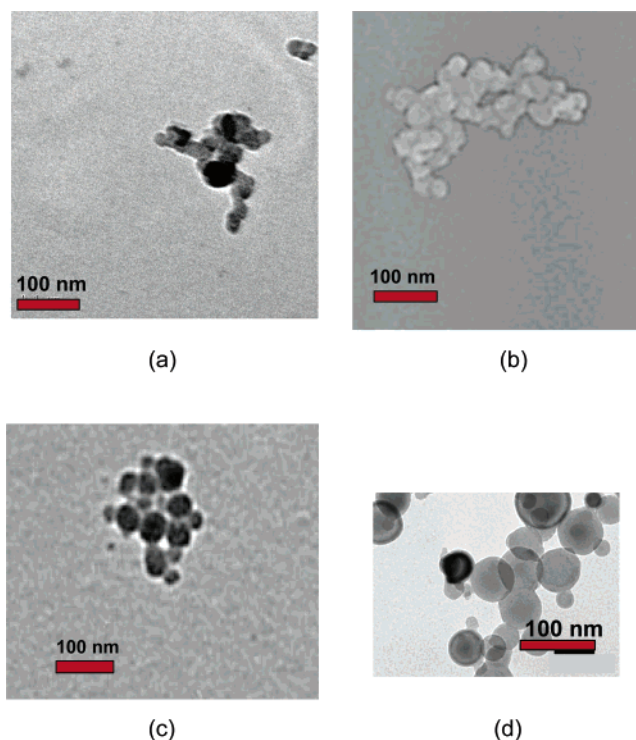
Diffusion controlled step:

$$\frac{t}{\tau_{\text{diffusion}}} = 1 - 3(1 - \alpha)^{2/3} + 2(1 - \alpha), \quad \tau_{\text{diffusion}} = \frac{\rho_{\text{Al}} D_{\text{p}}^{2}}{32 D_{\text{e}} C_{\text{O}_2,\infty}}$$

Chemical reaction controlled step:

$$\frac{t}{\tau_{\text{reaction}}} = 1 - (1 - \alpha)^{1/3}, \quad \tau_{\text{reaction}} = \frac{\rho_{\text{Al}} D_{\text{p}}}{8/3 k_{\text{s}} C_{\text{O}_2,\infty}} \quad (2)$$

where $t$ is the reaction time, $\rho_{Al}$ is the molar density of aluminum, $D_{\text{e}}$ is the effective diffusion coefficient of oxygen through the ash layer, $C_{\text{O}_2,\infty}$ is the oxygen molar concentration

in gas, $D_{\text{p}}$ is the particle diameter, and $k_{s}$ is the first-order rate constant for the surface reaction. To determine the rate-limiting step, we measured the extent of conversion by adjusting the reaction time ($t$) (i.e., the residence time in the furnace reactor) for a given temperature. By fitting each model (eq 2) to our experimental data ($t$ vs $\alpha$), we can infer the likely limiting step. Figure 11 plots our experimentally determined reaction time ($t$) and extent of conversion ($\alpha$) at 1100 °C for aluminum nanoparticles (Aveka Inc.), and a best fit to each reaction model. The results presented indicate that our experimental data are better fitted to the diffusion controlling model. Thus, we argue that two stages of reaction take place for aluminum nanoparticle oxidation: one where the shell of the aluminum oxide layer is quickly formed followed by the condensed phase diffusion limited reaction. Once the very thin layer is formed the kinetics may be controlled by diffusion. We have observed by TEM analysis that agglomerated Al particles retain their agglomerate structure after oxidation. The latter result is consistent with a model where the kinetics of oxide coating formation is fast relative to melting (and coalescence). Here we point out that readers may apply their own or better kinetic models to derive kinetic information using our raw data. In our previous study [17] we suggested that the phase change of the solid aluminum in the oxide shell may induce mechanical rupture, or the thinning of the oxide shell, and provide a route for transport of oxygen through the oxide shell, enhancing the diffusion rate through the oxide shell. In principle this mechanism does not necessarily counteract the model presented here as any cracking would also result in additional oxide formation, which would then serve as the diffusion barrier. In general, however, the shrinking core model may require further refinement as we learn more about the details of the early stage ignition process.

We are now in a position to extract a diffusion-limited rate constant and Arrehenius parameters (activation energy, pre-ex-

Aluminum Nanoparticle Oxidation

*J. Phys. Chem. B, Vol. 109, No. 15, 2005* **7297**
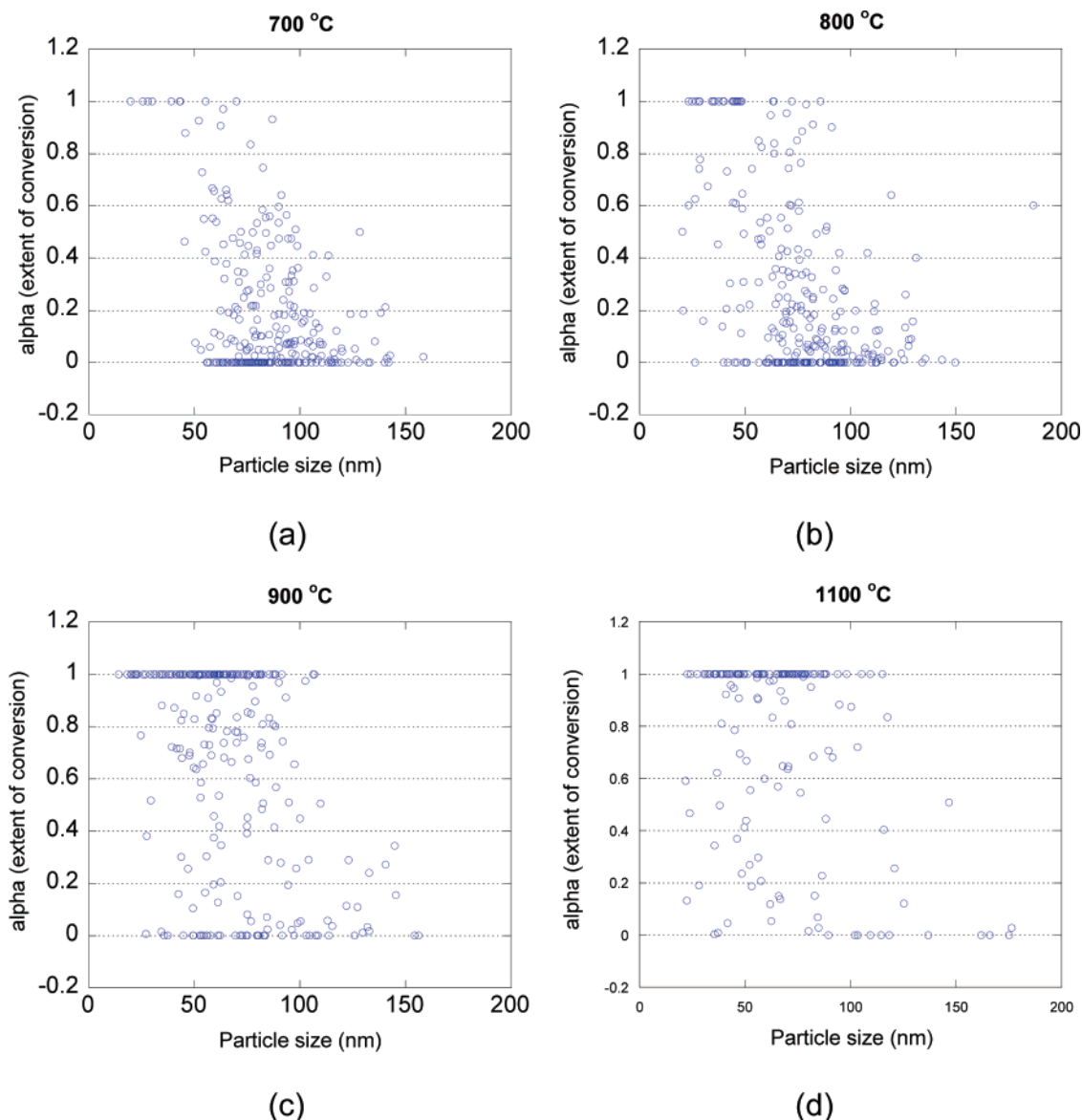
**Figure 10.** The extent of conversion ($\alpha$) as a function of particle size at each temperature for Al nanoparticles produced from the laser ablation method: (a) 700, (b) 800, (c) 900 °C, and (d) 1100 °C

**TABLE 1: Summary for Aluminum Nanoparticle Oxidation Measured with the SPMS**

| generation method | mean primary particle size[a] (nm) | peak mobility size[b] (nm) (mode diameter) | temp (°C) | fraction of completely oxidized particles (%) |
|---|---|---|---|---|
| DC Arc discharge | ~19 | ~65 | 900 | ~68 |
| laser ablation | ~23 | ~75 | 1100 | ~57 |
| nanopowder (Aveka) | ~29 | ~70 | 1100 | ~13 |
| nanopowder (Nanotechnologies) | ~50 | ~160 | 1100 | ~4 |

[a] The mean primary particle size was measured by using the TEM images. [b] The peak mobility size was measured with the scanning mobility particle sizer (SMPS).

ponential factor) using the shrinking core diffusion-controlled model as follows[3]

$$\frac{d\alpha}{dt} = k(T)f(\alpha), \quad k(T) = A \exp(-E_a/RT) \quad (3)$$

where the $k(T)$ is the rate constant, $f(a)$ is a mathematical representation of the reaction model, which can be obtained from the diffusion-controlled model shown in eq 2, $E_a$ is the activation energy, $A$ is the pre-exponential factor, and $T$ is the temperature. By using the average value of $\alpha$ (the extent of conversion) at each temperature as shown in Figure 8, we determined the

average rate constant as a function of temperature. Also, Arrehenius parameters (activation energy and pre-exponential factor) are obtained using the average rate constants and size-resolved (<50, 50–100, and 100–150 nm) rate constants as a function of temperature from Arrehenius plots (ln($k$) versus 1/$T$) as shown in Figure 12, parts a and b. Note that with decreasing particle size, the rate constant increased and the activation energy decreased. This might also be explained by the enhanced surface area-to-volume ratio with decreasing particle size discussed in the previous section. Table 2 summarizes Arrehenius parameters obtained from the size-resolved rate constants for Al particles produced from DC arc and laser ablation methods. It was

**TABLE 2: Summary for Arrehenius Parameters for Aluminum Nanoparticle Oxidation**

| generation method | particle mobility size (nm) | temp range (°C) | activation energy (kJ/mol) | pre-exponential factor (1/s) |
|---|---|---|---|---|
| DC Arc discharge | <50 | 600−900 | 31.8 | $2.4 \times 10^1$ |
| | 50−100 | | 56.9 | $1.8 \times 10^2$ |
| | 100−150 | | 174.6 | $5.4 \times 10^7$ |
| Laser ablation | <50 | 800−1100 | 24.6 | $3.5 \times 10^0$ |
| | 50−100 | | 104.8 | $5.0 \times 10^3$ |
| | 100−150 | | 120.2 | $4.4 \times 10^3$ |

consistently observed that the activation energy decreased with decreasing particle size. These results enable us to calculate the effective diffusion coefficients of oxygen through the ash layer using the rate constant as shown in eq 2, to give $D_e = 1.07 \times 10^{-9}$ (600 °C) to $1.31 \times 10^{-8}$ (900 °C) cm$^2$/s for DC arc generated aluminum nanoparticles of ~50 nm (i.e., $D_e = D_0 \exp(-E/RT)$, where $D_0 = 1.72 \times 10^{-5}$ cm$^2$/s and $E = 69.5$ kJ/mol over 600−900 °C).
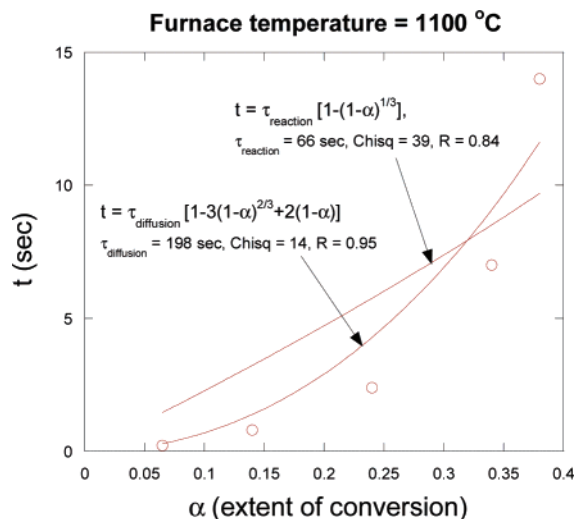
To provide a more physical picture of the reactivity of nanoparticles we compare the measured rate with the oxygen gas-collision rate[16] (i.e., the fastest possible oxidation rate).

$$\text{Theoretical collision rate (molecules/s)} = \frac{P_{O_2} \pi D_p^2}{(2\pi mKT)^{1/2}}$$

Measured reaction rate (molecules/s) =

$$-\frac{dN_{O_2}}{dt} = \frac{4\pi D_e}{\left(\frac{1}{r_c} - \frac{1}{R}\right)} C_{O_2} \quad (4)$$

where $P_{O_2}$ is the partial pressure of oxygen in gas, $m$ is the molecular mass of the gas molecules, $K$ is the Boltzmann's constant, $R$ is the particle size, and $r_c$ is the radius of unreacted core. The theoretical collision rate at 900 °C for 50 nm particles is ~$3.0 \times 10^{12}$ molecules/s, which is much greater than our experimental value (~$7.4 \times 10^5$ molecules/s).

One of the motivations in the use of the single-particle approach was to enable us to extract a more fundamental view of nanoparticle reactivity that was intrinsic to the particle and not influenced by ensemble effects or other effects associated with bulk methods. Here we compare kinetics extracted from
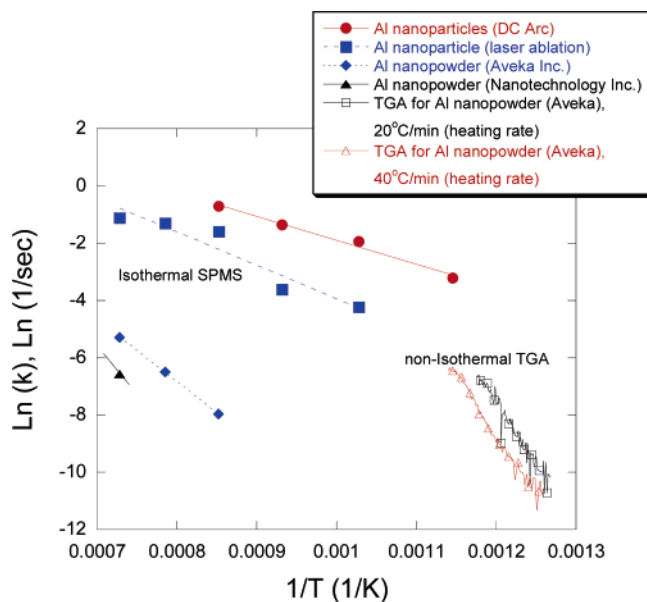
conventional non-isothermal thermal gravimetric measurements (TGA) with kinetic data obtained from the SPMS. The initial sample mass used in the TGA method was <1.0 mg of aluminum nanopowder (Aveka Inc.) with two different heating rates (20 and 40 °C/min) in a 20 cm$^3$/min flow of dry air. Using the extent of conversion that was evaluated through mass gain and the heating rate, we obtained reaction rates from the TGA data.[4] Figure 13 compares the TGA kinetic data with those obtained from the SPMS measurements. Despite the fact that we were unable to conduct both experiments in the same temperature regimes, it is quite apparent that for the same powder (Aveka) source, there are significant differences in the extracted rate between the two methods. The onset temperature for aluminum nanoparticle oxidation was found to be as low as 510−530 °C (below the melting point of aluminum) when the TGA method was used, while the SPMS results show that oxidation proceeds quickly above the melting point. In a prior study we have explored the role of phase transition to reactivity of aluminum[17] where we combined SPMS with high-temperature



(a)



(b)
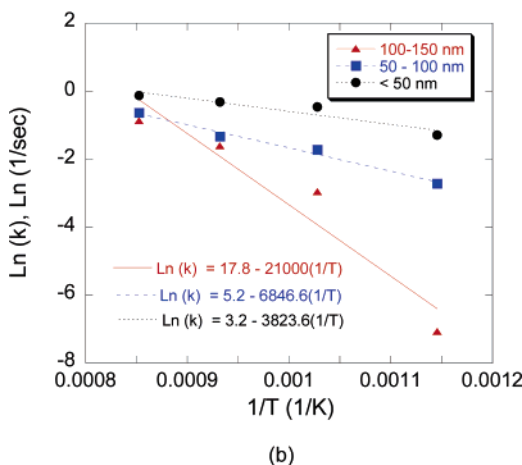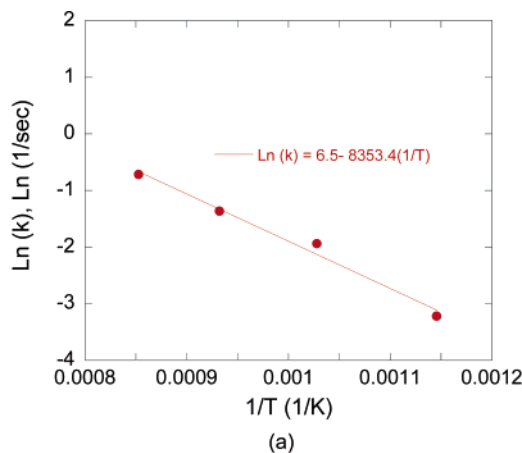
**Figure 12.** Arrehenius plots (ln ($k$) versus $1/T$) obtained from the average rate constants (a) and size-resolved rate constants (b) at each temperature for Al particles produced from the DC arc method; $k$ is the diffusion-limited rate constant and $T$ is the temperature (K).



**Figure 11.** The reaction time ($t$) and extent of conversion ($\alpha$) at 1100 °C for aluminum nanoparticles (Aveka Inc.) with the fitted lines determined by diffusion-controlled and chemical reaction-controlled shrinking core models; $\tau$ is the time for complete conversion for the diffusion-controlled or the reaction-controlled model.

Aluminum Nanoparticle Oxidation

*J. Phys. Chem. B, Vol. 109, No. 15, 2005* **7299**



**Figure 13.** Comparisons of kinetic data for aluminum nanoparticles obtained from the SPMS and TGA methods; $k$ is the diffusion-limited rate constant and $T$ is the temperature (K).

TEM to show that melting was necessary to induce stress fractures in the oxide coating that initiate subsequent oxidation. We hypothesize that the different oxidation characteristics obtained from these two techniques might be occurring because of the different initial sample masses ($\sim$1 fg for SPMS vs $\sim$1 mg for TGA), and residence times in the reactor ($\sim$1 s for SPMS vs 20 or 40 °C/min heating rate for TGA). This is consistent with the results of a prior study comparing[4] kinetics from SPMS vs TGA where we observed significant differences, which were attributed to heat and mass transfer effects for the bulk sample method. The errors due to these effects have been reported in the past.[3] The sample mass used in the SPMS was $\sim$1 fg (a single particle), as compared to sample size ($\sim$1 mg) used in the TGA. In other words, the TGA method used $\sim$$10^{12}$ particles packed in the bulk sample, while the SPMS used a single isolated particle in air. Since the oxidation reaction is highly exothermic, the amount of heat release from particles in the TGA can be quiet large. We argue that the heat release in the bulk sample would heat the particles above the pan temperature in the TGA and accelerate the reaction leading to a higher apparent reaction rate. This latter result and its consideration imply that caution should be given to kinetic measurements and on-set temperatures generated for materials where rapid reactions may lead to heat and mass transfer effects which corrupt the extraction of fundamental chemical kinetic rate parameters.

## IV. Conclusions

We applied a single particle mass spectrometer (SPMS) method to study oxidation and reactivity of aluminum nano-particles from a DC arc discharge, laser ablation, and commercial aluminum nanopowders. We found that the reactivity of aluminum nanoparticles increased with decreasing primary particle size and that the DC arc-generated aluminum nanoparticles that have the smallest primary particle size ($\sim$19 nm) were the most reactive. We found that the reactivity of aluminum nanoparticles was enhanced as particle mobility size decreased. We infer that this occurred because the surface area-to-volume ratio for Al agglomerates increased as particle mobility size decreased. Furthermore, based on the diffusion-controlled rate equation in the shrinking core model, we determined size-resolved rate constants and Arrehenius parameters (activation energy and pre-exponential factor). We found that the activation energy decreased as particle size decreased. For aluminum nanoparticles smaller than 50 nm, the activation energy was $\sim$32 (DC arc) to $\sim$25 kJ/mol (laser ablation), and increased to $\sim$175 (DC arc) and $\sim$120 kJ/mol (laser ablation) for particles in the size range of 100 to 150 nm. In addition, we observed that reaction rates measured with the SPMS were significantly different from those obtained from the conventional thermogravimetric analysis (TGA), which we attribute to artifacts inherent in the application of bulk thermal methods.

## References and Notes

(1) Ivanov, G. V.; Tepper, F. *4th Int. Symp. Spec. Top. Chem. Propul.* **1997**, 636.

(2) Aumann, C. E.; Skofronick, G. L.; Martin, J. A. *J. Vac. Sci. Technol. B* **1995**, *13* (3), 1178.

(3) Ortega, A. *Int. J. Chem. Kinet.* **2001**, *33*, 343.

(4) Mahadevan, R.; Lee, D.; Sakurai, H.; et al. *J. Phys. Chem. A* **2002**, *106*, 11083.

(5) Knutson, E. O.; Whitby, E. R. *J. Aerosol Sci.* **1975**, *6*, 443.

(6) Hering, S. V.; Friedlander, S. K.; Collins, J. J.; et al. *Environ. Sci. Technol.* **1979**, *13*, 184.

(7) Liu, P.; Ziemann, P. J.; Kittelson, D. B.; et al. *Aerosol Sci. Technol.* **1995**, *22*, 314.

(8) Murphy, D. M.; Thomson, D. S. *Aerosol Sci. Technol.* **1995**, *22*, 237. Noble, C. A.; Prather, K. A. *Mass Spectrom. Rev.* **2000**, *19*, 248. Suess, D. T.; Prather, K. A. *Chem. Rev.* **1999**, *99*, 3007. Johnston, M. V. *J. Mass Spectrom.* **2000**, *35*, 585. Kane, D. B.; Johnston, M. V. *Aerosol Sci. Technol.* **2001**, *34*, 520. Mahadevan, R.; Lee, D.; Sakurai, H.; et al. *J. Phys. Chem. A* **2002**, *106*, 11083. Jayne, J. T.; Leard, D. C.; Zhang, X.; et al. *Aerosol Sci. Technol.* **2000**, *33*, 49.

(9) Salt, K.; Noble, C. A.; Prather, K. A. *Anal. Chem.* **1996**, *68*, 230.

(10) Reents, W. D.; Ge, Z. *Aerosol Sci. Technol.* **2000**, *33*, 122.

(11) Reents, W. D.; Schabel, M. J. *Anal. Chem.* **2001**, *73*, 5403.

(12) Park, K. Ph.D. Thesis, University of Minnesota, 2003.

(13) Lee, D.; Park, K.; Zachariah, M. R. *Aerosol Sci. Technol.* Submitted for publication.

(14) Levenspiel, O. *Chemical Reaction Engineering*, 3rd ed.; John Wiley & Sons: New York, 1999.

(15) Yagi, S.; Kunii, D. *Chem. Eng. Sci.* **1961**, *16*, 364.

(16) Friedlander, S. K. *Smoke, Dust, and Haze*, 2nd ed.; Oxford University Press: New York, 2000.

(17) Rai, A.; Lee, D.; Park, K.; Zachariah, M. R. *J. Phys. Chem.* In press.